Custom Breast Phantom for an Accurate Tumor SNR Analysis

M. N. Cinti, R. Pani, *Member, IEEE*, F. Garibaldi, R. Pellegrini, M. Betti, N. Lanconelli, A. Riccardi, R. Campanini, G. Zavattini, G. Di Domenico, A. Del Guerra, *Senior Member, IEEE*, N. Belcari, W. Bencivelli, A. Motta, A. Vaiano, and I. N. Weinberg

***Abstract*—The capability of the scintimammography to diagnose subcentimeters sized tumors was increased by the employment of a dedicated gamma camera. The introduction of small field of view camera, based on pixellated scintillation array and position sensitive photomultiplier, allowed to enhance the geometric spatial resolution and contrast of the images due to reduced collimator-tumor distance.**

The aim of this paper is to investigate the realistic possibility of T1a tumors detection ($\sim$5 mm size) by comparing the signal-to-noise ratio (SNR) values obtained by different imagers. To this end, we have utilized a self-designed solid breast phantom with different sized hot spots (tumors). The phantom consists of seven disks with different thickness, molded from resin epoxy activated with Co^{57} isotope. The overlapped disks represent a pendula breast with about 800 cc volume. Hot spots have not wall. One disk has holes to fit the hot spots representing the different sized lesions. The imagers utilized were: a standard Anger Camera and three different cameras based on scintillator array, CsI(Tl) or NaI(Tl), coupled to position sensitive photomultiplier with different technologies, to make detectors with field of view of 3 and 5 inch. The experimental results are supported by Monte Carlo simulation. It was highlighted how spatial resolution is a predominant element in tumor visibility and how background causes a reduction of the image contrast. All gamma cameras show close results at SNR values less than 10 and a full detectability of 8 mm tumor size. However, the results show the 5 mm tumor size is lower detection limit for all cameras.

***Index Terms*—Biomedical nuclear imaging, photomultipliers, scintilation detectors.**

I. Introduction

SCINTIMAMMOGRAPHY capability to diagnose subcentimeter sized tumors was increased by the employment of dedicated gamma camera enables to acquire images of the breast comparable to the X-ray ones (cranio-caudal projection), also under compression [1]–[4]. The introduction of small field of view camera, based on scintillation array and position sensitive photomultiplier (PSPMT), allowed to enhance geometric spatial resolution and contrast of the images. These parameters are improved by the reduced collimator-tumor distance as a consequence of better positioning of the cameras.

The aim of this paper is to investigate realistic possibility of T1a tumors detection ($\sim$5 mm size) by comparing the signal-to-noise ratio (SNR) values obtained by different imagers. To this end, we have utilized a self-designed sliced solid breast phantom activated with Co^{57} isotope, with different sized hot spots (tumors). Overlapped disks represent a pendula breast with about 800 cc volume. The utilized imagers were a standard Anger Camera, a single photon emission gamma camera dedicated for scintimammography (SPEM) and two new cameras, based on new PSPMT generation and NaI(Tl) scintillator array. One is 2×2 array configuration of 1 inch PSPMT (Small Multiple Camera) and the other is based on Hamamatsu R8500 Flat Panel PSPMT (Flat Panel Camera).

The experimental results are supported by Monte Carlo simulation.

II. Equipment

A. SPEM, Small Multiple Camera, and Flat Panel Camera

The SPEM consists of a 5 inch Hamamatsu PSPMT R3292 coupled to same sized CsI(Tl) scintillating array with $2 \times 2 \times 3$ mm^3 individual pixel size. Detailed description of the SPEM camera is reported elsewhere [4].

Small multiple camera (SMC) [5] is a multiple camera and consists of 4 PSPMT Hamamatsu R7600-C8 [6] in 2×2 array configuration coupled to a NaI(Tl) pixellated scintillator ($1.8 \times 1.8 \times 3$ mm^3 pixel) with 3 mm glass window. High scintillation efficiency of the NaI(Tl), combined with the glass window, allowed to balance the effects of the dead zone between the PSPMTs. The Hamamatsu R7600-C8 PSPMT (bialkali photocathode) is a compact, metal channel dynode photomultiplier with readouts by wire anodes $(4X + 4Y)$. The active area is 22×22 mm ^{2} and the overall dimensions are $26 \times 26 \times 20$(h) mm^3. Each wire anode is directly connected to a preamplifier and a weighted summing circuit computes the charge distribution centroid. The acquisition system consists of an analog-digital converter (ADC) module (FAST 7074) connected to a multiparameter acquisition card, inside a Pentium personal computer operating in Windows environment (FAST

Manuscript received April 1, 2003; revised July 28, 2003. This work was supported in part by the MIUR Cofin 2000 Project.

M. Nerina Cinti is with the Biophysics Ph.D. School, University of Rome "La Sapienza", 6-00161 Rome, Italy (e-mail: marianerina.cinti@uniroma1.it).

R. Pani, R. Pellegrini, and M. Betti are with the Department of Experimental Medicine and Patology, University of Rome "La Sapienza", 6-00161 Rome, Italy.

F. Garibaldi is with the Laboratory of Physics, ISS-00163 Rome, Italy.

N. Lanconelli, A. Riccardi, and R. Campanini are with Department of Physics, University of Bologna, 40126 Bologna, Italy.

G. Zavattini and G. Di Domenico are with Department of Physics, University of Ferrara, 4100 Italy.

A. del Guerra, N. Belcari, A. Motta, and A. Vaiano are with Department of Physics, University of Pisa, 56126 Pisa, Italy.

W. Bencivelli is with Department of Internal Medicine, University of Pisa, 56126 Pisa, Italy.

I. Weinberg is with PEM Technologies, Bethesda MD 20187 USA.

Digital Object Identifier 10.1109/TNS.2004.824827

MPA/WIN). The multiparameter system was able to control up to eight ADCs with a maximum count rate of 400 KHz. The maximum electronics count rate was 30 KHz. The data were acquired in list mode through a 1 Mbyte first-in-first-out register inside the MPA card. We developed software to process and elaborate data for the image analysis in Interactive Data Language (IDL) environment.

The same NaI(Tl) pixellated scintillator was also coupled to a flat panel PSPMT Hamamatsu R8500 [7]. This PSPMT has external size of $51.7 \times 51.7 \times 12.4$ mm^3, the photocathode is bialkali and 12 stages metal channel dynode are used as electron multiplier. 8×8 anode matrix is used for position sensitive function in which each individual anode is 6 mm sized. Peripheral dead zone is reduced down to 1 mm, so the overall active area is 49.7 mm squared. The photomultiplier (PMT) gain is about $3 * 10^6$, and the glass window thickness was 2 mm. A multianode read out technique [8] was used in which the charge on each anode is individually acquired and digitized. The subsequent position calculation is performed in software. Chip outputs may be read out sequentially on a single channel. The serial output is subsequently read by a 1.5 MHz National Instruments 6110E ADC mounted in host computer.

It is essential to emphasize the differences between imagers dimension: if Anger camera and SPEM are fixed, heavy, the FPC, and SMC are smaller and, on consequence, more suitable, with the appropriate size and positioning, to arrange different detection areas.

Imagers performances were tested with a general purpose (type A) and an high efficiency collimator (type B) whose characteristics are summarized in Table I.

TABLE I
COLLIMATOR CHARACTERISTICS

Camera	Collimator	Sensitivity	Spatial Resolution FWHM SCD (@10 cm)	Hole Φ (mm)	Hole Length (mm)	Septa Thick (mm)
Anger	G.E. General Purpose H2503DF	362 cpm/μCi[a]	9	2.5	41	0.3
SPEM SMC FPC	General Purpose (type A)	327 cpm/μCi[b]	8.8	1.5	22	0.2
SPEM FPC	High Efficiency (type B)	1912.75 cpm/μCi[b]	17.39	3	25	0.3

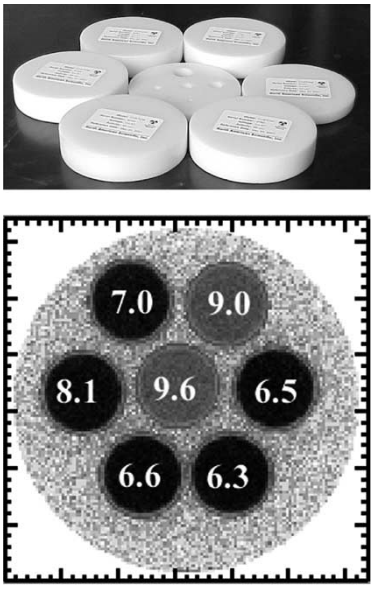

Fig. 1. Upper, phantom single slides and lower, its image in Anger camera. The numbers represent the percentage counting uniformity. The lighter disks correspond to the 1 cm slide thick.

B. Breast Phantom

Solid breast phantom consists of seven disks (five slabs with 2 cm thickness and 2 slabs with 1 cm thickness) with (9.0 ± 0.1) cm diameter. The overlapped disks represent a pendula breast of about 800 cc volume. Disks are molded from epoxy resin, activated with Co^{57} isotope, with $1.079 \pm 5\%$ (g/cc) density. Activity density of the breast phantom was fixed at 500 nCi/cc, a 5:1 ratio respect to clinical breast activity, in order to reduce detection time and to counterbalance short half-life of the ^{57}Co source. The phantom photo is showed in Fig. 1 (upper). The slabs have been tested with an Anger camera in order to evaluate the counting uniformity. In Fig. 1 (lower) the slabs image by the Anger camera are reported where the lighter disks represent the 1 cm slabs (see Fig. 1 upper for reference); the values of the percentage counting uniformity are indicated. For safety reason, each disk is enveloped into thin plastic shell ($\sim$1 mm thick). A 1 cm disk contains holes with the same size of hot spots (hot spot support). The holes can be filled both with hot spots or with plugs having the same radioactive concentration and density of the breast. A no-activated copy of breast phantom was made to implement the measurements.

C. Hot Spots

Hot spots geometry was designed to simulate tumor size ranging between T1a to T1c tumor clinical classification and they have not wall to simulate the exact dimension of real lesion. Fig. 2 shows support disk and hot spots. The hot spot:breast uptake is 10:1 [9], [10].

III. MEASUREMENTS AND ANALYSIS METHOD

The measurements were performed both in prone and craniocaudal projections, to follow possible clinical setting, as it is shown in Fig. 3. The sliced breast phantom allows to study imagers response as function of breast thickness and tumor position. The image correction was performed by a lookup table (LUT) procedure from flood field irradiation of all camera (for details see A paragraph). Data acquisition time were corrected considering ^{57}Co decay time to collect statistically comparable counts per image.

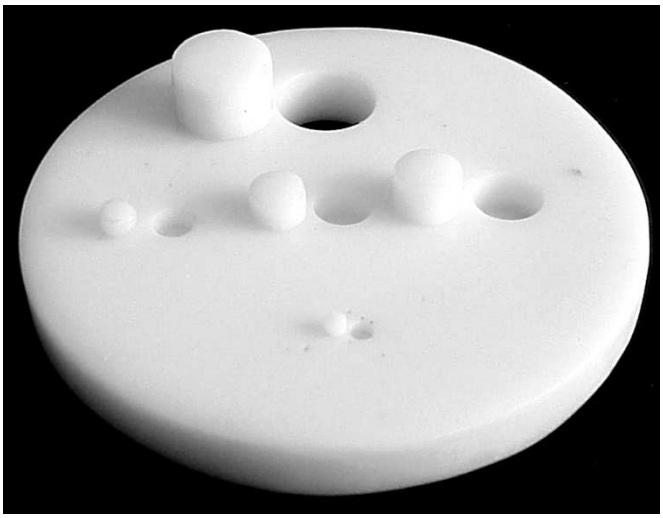

Fig. 2. Tumor support slide and tumors.

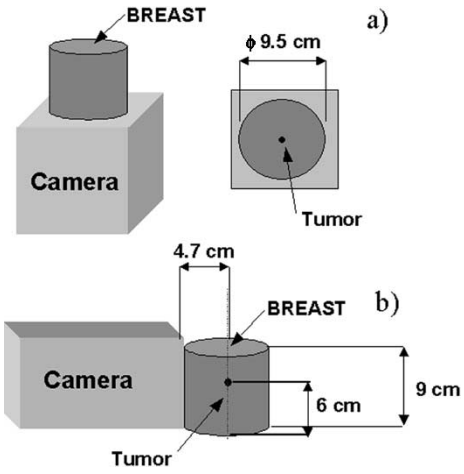

Fig. 3. (a) Cranio caudal and (b) prone projection measurement sketch.

The method consists in evaluating tumor SNR as function of imager, dimension of the breast, lesion position, and dimension and tumor/background uptake. SNR is defined as [11]–[14]

$$\mathrm{SNR} = \frac{\Sigma - \mathrm{BKG}}{\sqrt{\Sigma}} \tag{1}$$

where Σ is counts sum on the Region of Interest (ROI), containing the tumor, while BKG is the media on counts of a background ROI with the same dimension of tumor one. Background and tumor images were collected separately and the final images were performed matching the two kind of image. Tumor image is obtained inserting investigated tumor in no active phantom copy, at fixed breast thickness and source collimator distance. Background image consists in the image coming from the ovelapping appropriate number of slabs, simulating the fixed breast thickness. The SNR study as function of tumor:breast uptake was performed changing tumor image acquisition time, proportionally to the requested uptake.

Finally, we associated to phantom images another parameter, the image contrast (IC), to link with SNR, in order to foresee a trend which characterizes imagers behavior. We approach the image contrast IC in term of "luminosity" of the source (tumor) and so we utilized the definition [14]–[16]

$$\mathrm{IC} = \frac{\mathrm{Max} - \mathrm{BKG}}{\mathrm{Max}} \tag{2}$$

where Max is the maximum counts value between the pixel in tumor ROI and BKG is the media of background counts. In this definition the IC value theoretically raging between 0% to 100%.

IC and SNR values are calculated on images corrected by LUT.

A. Lookup Table

In the pixellated gamma camera, the uniformity of pulse height response affects the overall energy resolution and the energy window selection. To correct the image, we created a LUT using flood field irradiation images of the detectors. These images were obtained by a Co^{57} flood field source (351 μCi @ 5/21/2001), 15 cm diameter, positioned on the collimator plane. The LUT procedure is based on the generation of three matrixes: a position linearity matrix, which redistributes spatially the events in order to rebuild the pattern of the scintillator array; the realization of this matrix is based, where possible, on pixel identification (for example in FPC and SMC). The second one is a matrix of the gain factors to rechannel the spectra corresponding to each crystal; the last one is a matrix made by the resulting homogeneous counting coefficients inside an energy window in order to select only the photopeak events [17]

B. Montecarlo Simulation

The Monte Carlo code used is EGSnrc, latest version [18]. The simulated phantom is similar to the one really used: the only differences is that the simulated hot spot are spherical rather than cylindrical. The mentioned distances are considered from the center of the sphere to the surface of the camera. The collimator is a general purpose with the same characteristic reported on the Table I and also scintillator lattice death zone was inserted to make the simulation as close to reality as it is possible. The set scintillator is a CsI(Tl) array, $2 \times 2 \times 3$ mm^3 pixel. Simulations include all the physical processes available with EGS, as Compton and Rayleigh scattering, photoelectric absorption with emission of fluorescence photons or Auger electrons. The lower cutoff energy is fixed to 5 keV for photons, whereas electron transport was neglected (an electron deposits all its energy in the point of interaction). These assumptions hold in the entire simulated apparatus: in the breast phantom, in the collimator and in the detector. The simulation follows the same way as the measurement in considering lesions and background divided.

IV. Results

The profiles coming from SPEM, SMC and FPC camera, obtained by a flood field irradiation, are reported in Fig. 4. As it is clearly visible, pixel identification strongly improves coming from SPEM to SMC and FPC. The poor pixel identification for the SPEM, visible in Fig. 4(a), involves a poor counting homogeneity, due to an intrinsic response unhomogeneity of the

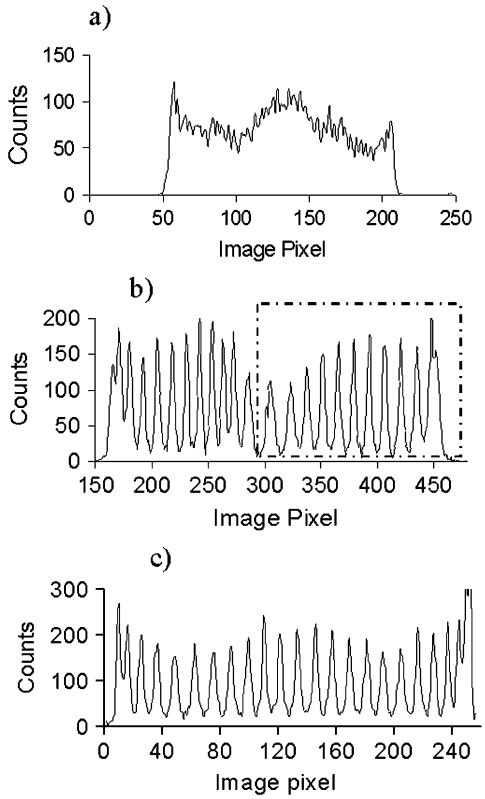

Fig. 4. (a) SPEM (10 cm FOV); (b) SMC (5 cm FOV); and (c) FPC (5 cm FOV) cross section of flood field image. In (b) the box represents the camera area used to evaluate the SNR.

TABLE II
DETECTOR PERFMORMANCES

Detector	Peak/Valley (mean value)	Position Response (mean dev.) channel	Counting Response (E-window)* SD %	Photofraction* %	Spatial Resolution FWHM (mm)	Energy Resolution* %
ANGER	-	-	4.0	75.0	3.5[a]	11.0
SPEM	1.1	±7.5	48.0	60.0	1.7[b]	21.0
SMC	9.2	±5.5	29.2	40.4	0.8[b]	12.3
FPC	9.0	±2.5	10.0	61.3	0.9 [b]	12.0

detector, verifiable in Table II where we report the principal features of each cameras.

Best values in term of counting uniformity and photofraction are obtained for SMC and FPC, obtained after LUT procedure application. These results shown how LUT procedure depends on pixel identification and peak/valley ratio, parameters that for SMC and FPC are better. Obviously, the poorer counting response of the SMC in dead zone between PSPMTs, introduced by multiple configuration, penalizes this camera respect to the FPC.

To compare the image dimension of a T1b (8 mm) tumor, respect to imager FoV, we show in Fig. 5 the 8 mm tumor images for all cameras, 3 cm tumor depth, 3 cm breast thickness and 50:1 uptake, after LUT correction.

In Fig. 6 we present the SNR results obtained for different tumor/background uptake for 5 mm tumor size, in two breast phantom configuration. In the case of 3 cm tumor depth, 3 cm breast thickness (Fig. 6 upper), all the cameras are under visibility limit for uptake lower than 10:1 and all SNR values are

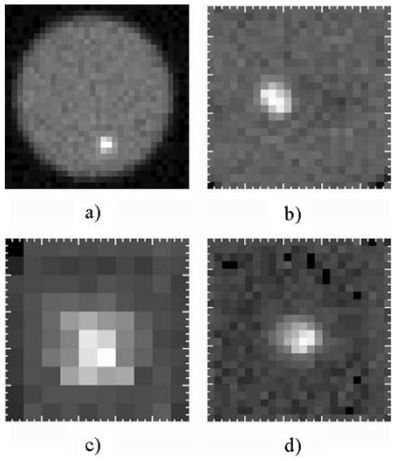

Fig. 5. 8 mm tumor images for all cameras, 3 cm tumor depth, 3 cm breast thickness and 50:1 uptake. (a) Anger camera. (b) SPEM. (c) SMC. (d) FPC.

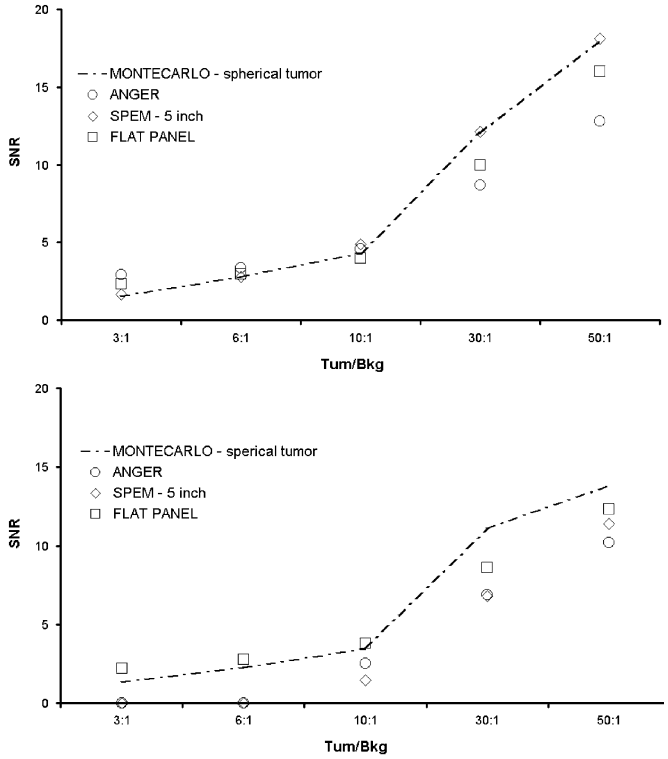

Fig. 6. SNR value versus uptake for 5 mm tumor size. Upper: 3 cm tumor depth, 3 cm breast thickness. Lower: 3 cm tumor depth, 6 cm breast thickness.

very close. For higher uptake (30:1, 50:1) SNR values become apart; SPEM values are higher than FPC and Anger ones. In 3 cm tumor depth, 6 cm breast thickness condition (Fig. 6 lower) we obtained different results: SPEM SNR values decrease and FPC results the best imager even if MC values are always higher. Relating the two situations, the importance of the camera positioning (lesion-collimator distance) is highlighted as one of the main factors to the small tumor detection.

Breast background is another important factor affecting SNR, in particular 6 cm breast thickness represents the most critical condition for all gamma cameras to detect 5 mm tumor. For 8 mm tumor (see Fig. 7), it is shown how SPEM SNR values are under the other cameras ones; the FPC becomes dominant

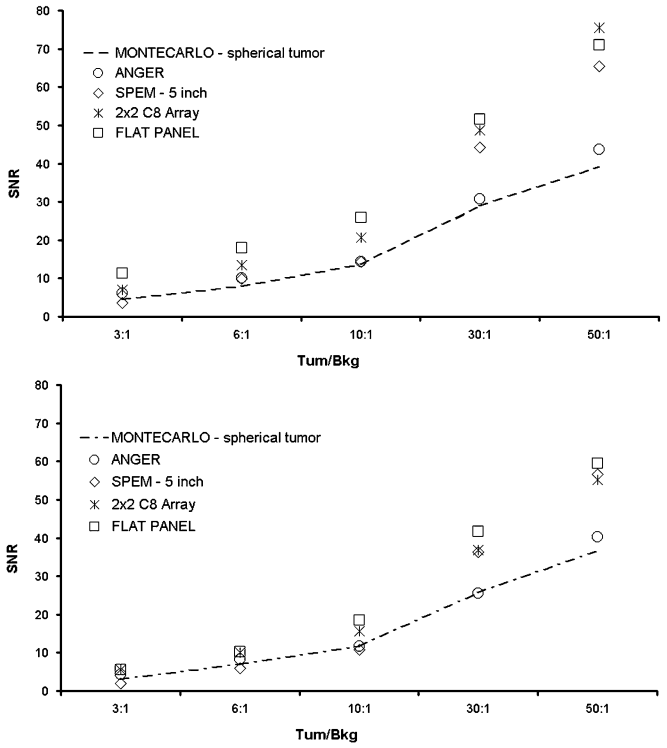

Fig. 7. SNR value versus uptake for 8 mm tumor size. Upper: 3 cm tumor depth, 3 cm breast thickness. Lower: 3 cm tumor depth, 6 cm breast thickness.

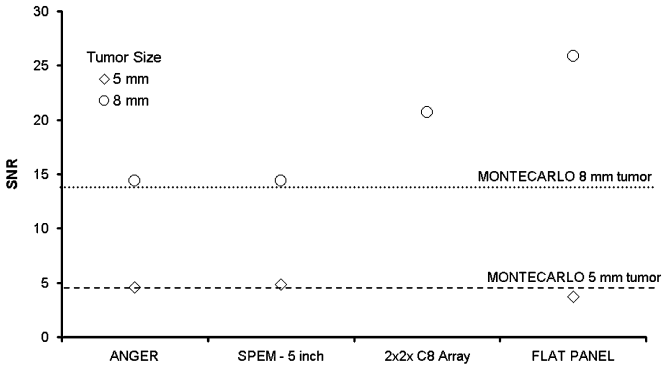

Fig. 8. SNR value versus cameras for 5 mm and 8 mm tumor size, 3 cm tumor depth, 3 cm breast thickness.

in both 3 cm tumor depth, 3 cm breast thickness and 3 cm tumor depth, 6 cm breast thickness. In the first situation, yet at 6:1 uptake all values are over visibility limit. Gamma cameras with very high intrinsic spatial resolution and good pixel identification (PID) show better performances at high SNR values (greater 20).

In Fig. 8 it is shown a summarizing behavior of all cameras for 5 mm and 8 mm tumor for 3 cm tumor depth and 3 cm breast thickness, in 10:1 uptake condition., compared to Montecarlo results. The results show how there are not significant differences amongst different cameras for 5 mm tumor, while for 8 mm tumor FPC and SMC are strongly over the other values, resulting to be the best imagers for T1b tumor.

To complete the scenario of the possible clinical trials, in Fig. 9 we present the results obtained by a 8 mm tumor size, in prone projection (6 cm tumor depth, 9 cm breast thickness).

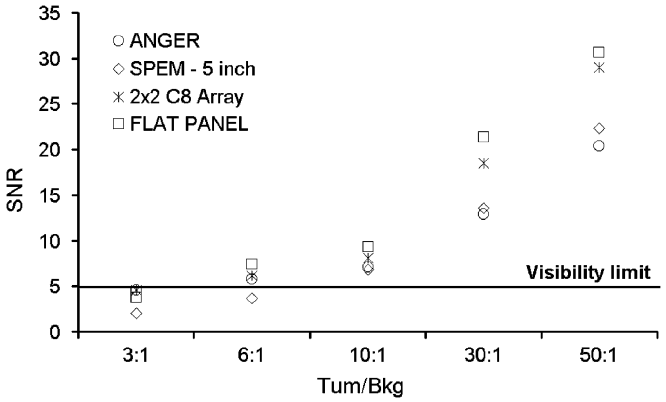

Fig. 9. SNR value versus uptake for 8 mm tumor size, 6 cm tumor depth, 9 cm breast thickness, prone projection.

TABLE III
CONTRAST VERSUS SNR FIT RESULTS
$[\mathrm{CONTRAST} = \mathrm{M} * \mathrm{LN}(\mathrm{SNR}) + \mathrm{Q}]$

Phantom Configuration	m ± σ	q ± σ	χ^2
5 mm tumor - 3 cm depth,	0.24 ± 0.03	0.00	0.2
3 cm breast thick (Fig. 10a)	0.14 ± 0.03	0.040 ± 0.004	0.2
8 mm tumor, 3 cm depth,	0.23 ± 0.02	-0.14 ± 0.02	0.2
3 cm breast thick (Fig. 10c)			
8 mm tumor, 3 cm depth,	0.26 ± 0.03	-0.19 ± 0.02	0.8
6 cm breast thick (Fig.10d)	0.18 ± 0.02	-0.080 ± 0.001	1

The values confirm foreseen poor tumor detection, due to large tumor-collimator distance and breast thickness greater than 6 cm, also for 10:1 tumor/breast uptake, in prone position. Analysis of image contrast linked with SNR in semi logarithmic scale. Each experimental point is obtained changing tumor/background uptake (3:1, 6:1, 10:1, and 50:1). The visibility limit, was set in terms of SNR, to 5 (horizontal lines). The lesions considered are 5 and 8 mm size. To better understand the results, it is necessary to make a preamble: camera counting unhomogeneity could affect image contrast because it depends on selected point position, but it does not affect SNR in which tumor ROI counts media rather than maximum value is considered. This element be becomes relevant during small lesion analysis, where the relative image are affected by a low statistic.

Starting by Fig. 10(a), we show the Contrast versus SNR, for a 5 mm tumor, 3 cm tumor depth, 3 cm breast thickness. Two trends are visible: the higher one consists in data coming from FPC and MC simulation, the other coming from SPEM and ANGER camera. On the graph we report the fitting lines which represent the two trends; in Table III, first row, there are the relative fit coefficients which follow the law:

$$\mathrm{IC} = \mathrm{m} * \ln(\mathrm{SNR}) + \mathrm{q}. \tag{3}$$

In this case spatial resolution is dominant, which defines the two class of imagers in term of IC; anyway the Anger response is not adequate. The superior limit in figure, indicates the values for 5 mm tumor size, 0 cm depth, 3 cm breast thickness, flat panel camera, 50:1 uptake. In Fig. 10(b) it is shown the contrast versus SNR for a 5 mm tumor, 3 cm tumor depth, 6 cm breast thickness. We are treating low SNR and contrast values, on

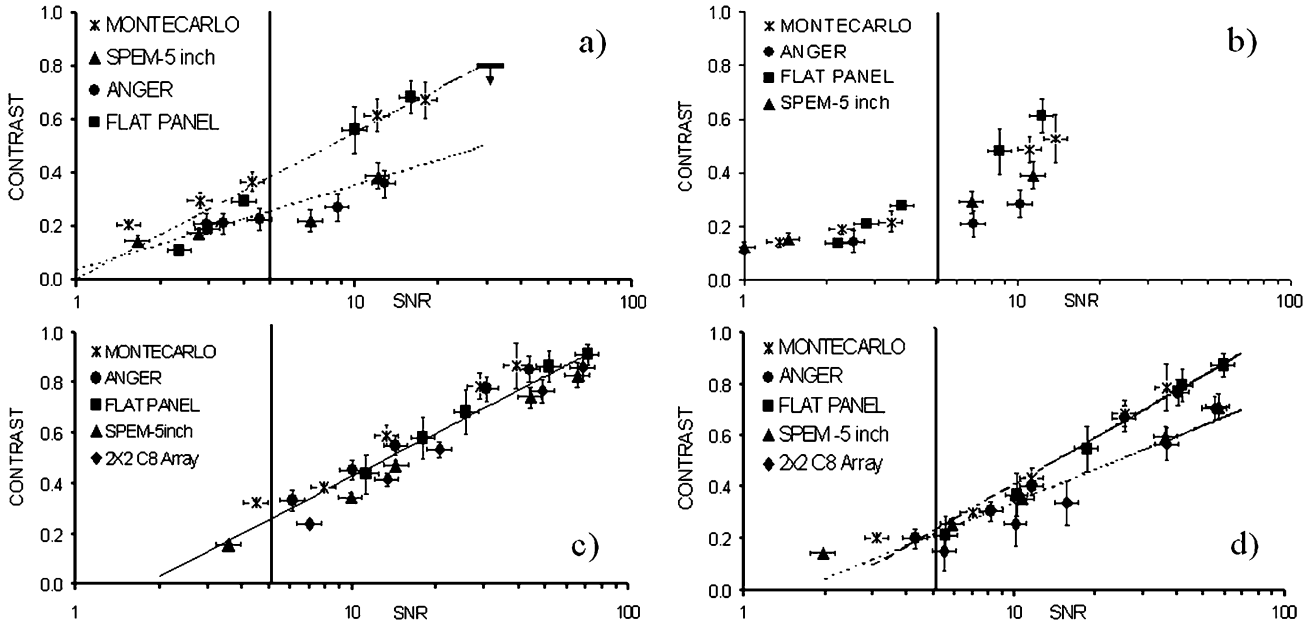

Fig. 10. Contrast versus SNR, for different breast phantom configuration. The points represent values obtained at different tumor/bkg uptake (3:1, 6:1, 10:1, 30:1, and 50:1). The collimator was a general purpose (type A). The solid horizontal line shows the SNR visibility limit. (a) 5 mm tumor, 3 cm depth, 3 cm breast thickness. (b) 5 mm tumor, 3 cm depth, 6 cm breast thickness. (c) 8 mm tumor, 3 cm depth, 3 cm breast thickness. (d) 8 mm tumor, 3 cm depth, 6 cm breast thickness.

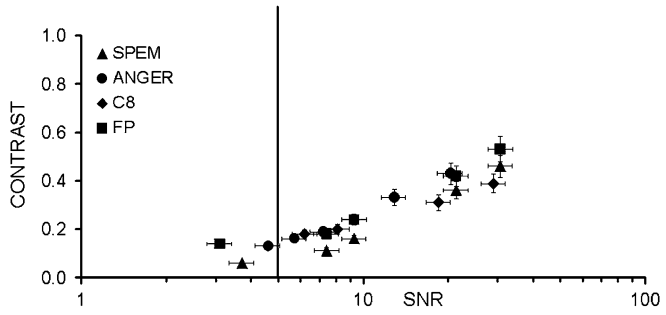

Fig. 11. Contrast versus SNR, 8 mm tumor size, prone position.

consequence the main part of the data are close down the visibility limit, indicating that in this condition the 5 mm tumor is not detectable for uptake less than 20:1.

In Fig. 10(c) we show the contrast versus SNR, for a 8 mm tumor, 3 cm tumor depth, 3 cm breast thickness. The data seem to follow an unique trend which confirmed that in case of very good tumor visibility (from 6:1 uptake for all cameras) there are no substantial differences between the imagers. The fit coefficients are reported in Table III, row 2.

Finally, in Fig. 10(d), we show the contrast versus SNR, for a 8 mm tumor, 3 cm tumor depth, 6 cm breast thickness. Also in this case, two trends are visible: the higher one consists in data coming from FPC, ANGER, and MC simulation, the other one in data coming from SPEM and SMC. In this phantom configuration, an higher background supports the imagers with better counting homogeneity than with high spatial resolution and so Anger camera presents IC values better than SPEM.

The fit coefficient are reported in Table III, row 3. Comparing the angular coefficients between the first and third row, it is clear how the two class of detector follow the same trend in two different conditions. In Fig. 11 it is shown the contrast versus SNR,

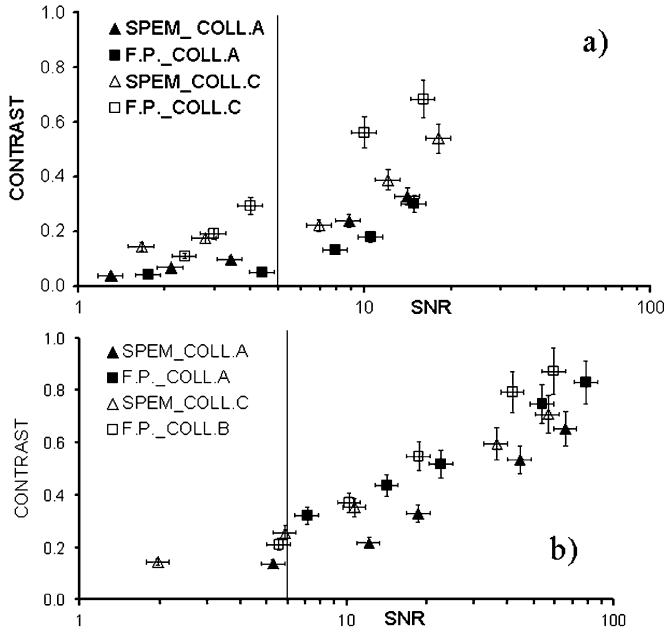

Fig. 12. Contrast versus SNR versus collimator. (a) 5 mm tumor size, 3 cm breast, 3 cm breast thickness. (b) 8 mm tumor size, 3 cm breast, 6 cm breast thickness.

for a 8 mm tumor size, prone position. The imager have a very close behavior but all IC values are lower than 60% confirming the poor tumor detection in this situation.

Finally, we compare the performances of SPEM and FPC with two different collimator (type A and B, see Table I). In Fig. 12 we show the contrast versus SNR, for two phantom configuration: a) 5 mm tumor size, 3 cm breast thickness, 3 cm tumor depth and b) 8 mm tumor size, 6 cm breast thickness, 3 cm tumor depth.

V. Conclusion

From the IC versus SNR behavior, it is highlighted how two class of imagers are presented. They are defined by two trends depending on which one it is the most important imager characteristic that affects tumor visibility, relating to phantom configuration. According to the dominant factor, spatial resolution or counting uniformity response, the cameras presenting better value of this parameter are on the higher trend. For 5 mm tumor size, all cameras present low results until 20:1 uptake, for the phantom configuration with high background (6 cm thick).

As in breast spot compression situation (3 cm thick), the spatial resolution becomes the most important factor and on consequence FPC results the best, confirming the Montecarlo data. In any case, Anger camera spatial resolution is a not adequate to reveal 5 mm tumor size. In conclusion, 5 mm tumor size represents the lowest detection limit for all cameras, for present clinical uptake.

For 8 mm tumor size, counting uniformity response is the dominant parameter, because of the high tumor visibility in all imagers. In fact, for small background thickness (3 cm), only one trend is presented, confirming that tumor size detection is not affected by considered cameras spatial resolution. On the other hand, for 6 cm background, the cameras IC seems to be dominated by counting uniformity response.

Low IC values obtained in prone position measurements confirmed the necessity to operate in cranio-caudal position for clinical trial to improve spatial resolution and to minimize breast background.

High efficiency collimator, even if it improves the image statistic doesn't improve the IC respect to a general purpose one. So the last one seems to be the best tradeoff to implement tumor visibility.

References

[1] D. Steinbach, S. Cherry, N. Doshi, A. Goode, B. Kross, S. Majewski, A. G. Weinsenberger, M. Williams, and R. Wojcik, "A small scintimammography detector based on a 5″ PSPMT and a cristall scintillator array," in *Proc. IEEE Nuclear Science Symp. 1997*, vol. 2, Albuquerque, NM, Nov. 9–15, 1997, pp. 1255–1259.

[2] M. B. Williams, A. R. Goode, V. Galbis-Reig, S. Majewski, A. G. Weinsenberger, and R. Wojcik, "Perfomrance of a PSPMT based detector for scintimammography," *Phys. Med. Biol.*, vol. 45, pp. 781–800, 2000.

[3] Z. He, A. J. Bird, D. Ramsden, and Y. Meng, "A 5 inch diameter position sensitive scintillation counter," *IEEE Trans. Nucl. Sci.*, vol. 40, pp. 447–451, 1993.

[4] R. Pani *et al.*, "Dedicated gamma camera for single photon emission mammography (SPEM)," *IEEE Trans. Nucl. Sci.*, vol. 45, Dec. 1998.

[5] R. Pani *et al.*, "Portable gamma camera for clinical use in nuclear medicine," in *Proc. IEEE Nuclear Science Symp. Conf. Rec.* , vol. 2, Anahiem, CA, 1996, pp. 1170–1174.

[6] "R7600-C8 Position Sensitive Photomultiplier ," Hamamatsu Tech. Data Sheet, Hamamatsu City, Japan, 1994.

[7] "R8500 Flat Panel Position Sensitive Photomultiplier," Hamamatsu Tech. Data Sheet, Hamamatsu City, Japan, 1994.

[8] "HX2/RAL/SS System Readout," Rutherford, Appleton Labs. Microelectron. Group Tech. Data Sheet, Chilton-Didcot, Oxfordshire, U.K., 1995.

[9] J. Maublant, M. de Latour, D. Mestas, A. Clemenson, S. Charrier, V. Feillel, G. L. Bouedec, P. Kaufmann, J. Dauplant, and A. Veyer, "Technetium-99 m-sestamibi uptake in breast tumor associated lymph nodes," *J. Nucl. Med.*, vol. 37, pp. 922–925, 1996.

[10] S. Majewski *et al.*, "Optimization of dedicated scintimammography procedure using detector prototypes and compressible phantoms," *IEEE Trans. Nucl. Sci.*, vol. 48, pp. 822–829, June 2001.

[11] J. M. Tapiovaara and R. F. Wagner, "Snr and noise measurements for medical imaging. I. A practical approach based on statistical decision theory," *Phys. Med. Biol.*, vol. 38, pp. 71–92, 1993.

[12] G. J. Gruber, W. W. Moses, and S. E. Derenzo, "Montecarlo simulation of a breast tumor imaging properties with compact, discrete gamma cameras," *IEEE Trans. Nucl. Sci.*, vol. 46, pp. 2119–2123, Dec. 1999.

[13] G. De Vincentis *et al.*, "Results of clinical trias with SPEM," *NIMA*, vol. 497, pp. 46–50, 2003.

[14] M. Z. Kiss, D. E. Sayers, and Z. Zhong, "Measurement of image contrast using diffraction enhanced imaging," *Phys. Med. Biol.*, vol. 48, pp. 325–340, 2003.

[15] H. E. Johnes, *The Physics of Radiology*. Springfield, IL: Charles C. Thomas, 1964.

[16] M. Zanarini *et al.*, "Contrast evaluations in a digital mammographyc system," in *Proc. IEEE NSS Conf. Rec.*, vol. 2, Toronto, ON, Canada, Nov, 8–14, 1998, pp. 1300–1304.

[17] M. N. Cinti, R. Pani, R. Pellegrini, C. Bonifazzi, R. Scafè, G. De Vincentis, F. Garibaldi, F. Cusanno, R. Campanini, N. Lanconelli, A. Riccardi, and A. del Guerra, "Tumor SNR analysis in scintimammography by dedicated high contrast imager," *Trans. Nucl. Sci.*, pp. 1618–1623, Oct. 2003.

[18] B. D. Bollini, R. Campanini, M. Gombia, N. Lanconelli, and A. Riccardi, "A modular description for collimator geometry in EGS simulation tasks," *Proc. IEEE NSS-MIC Conf. Rec.*, vol. 3, pp. 1303–1305, Nov. 4–10, 2000.